Desalination and Water Treatment
www.deswater.com

doi: 10.5004/dwt.2018.22225

110 (2018) 76–88
April

Performance and fouling behaviors in a membrane-assisted biological nutrient removal process with focus on the effect of influent COD/N ratio

Zhaozhao Wang[a,b], Ying Ji[a,b], Lina Yan[c], Dan Zhao[a,b], Kai Zhang[a,b], Wei Zhang[a,b], Simin Li[a,b,*]

[a]*College of Energy and Environmental Engineering, Hebei University of Engineering, Handan 056038, China, Tel. +8618303233729; emails: 18303233729@163.com (S. Li), w-z-z@163.com (Z. Wang), 18244606382@139.com (Y. Ji), 18732059211@163.com (D. Zhao), hebeizuiqingfeng@163.com (K. Zhang), zhangwei1981@hebeu.edu.cn (W. Zhang)*
[b]*Center for Water Pollution Control and Water Ecological Remediation, Hebei University of Engineering, Handan 056038, China*
[c]*Graduate Department of Hebei University of Engineering, Handan 056038, China, email: yanlina01@126.com (L. Yan)*

Received 31 October 2017; Accepted 9 March 2018

ABSTRACT

A bench-scale University of Cape Town-membrane bioreactor was utilized to treat synthetic municipal wastewater with focus on the effect of chemical oxygen demand (COD)/total nitrogen (TN) (COD/N) ratio on biological nutrient removal and membrane fouling behaviors. The process showed a strong capability of anti-shock organic loading, and an average 89.9% removal efficiency of organic matter was achieved, indicating that COD removal was independent of the COD/N ratio. The average removal efficiencies of TN and total phosphorus (TP) were highest at a COD/N ratio of 7.3 at 90.3% and 92.4%, respectively. The proportions of TN removal via simultaneous nitrification and denitrification (SND) and TP removal via anoxic phosphorus removal increased to 27.9% and 44.91% from 1.6% and 7.94% (COD/N ratio of 3.2), respectively. A higher fouling rate was observed with increasing COD/N ratio, due to the changes in the nitrogen removal pathway. The increase of organic loading and decrease of dissolved oxygen induced SND behavior that affected the physiochemical properties and metabolic productions of the aerobic biosolids. The sludge filterability deteriorated due to the higher bound extracellular polymeric substances and soluble microbial products that were produced under SND condition, which also resulted in a higher modified fouling index both for suspended solids and soluble components. Biofloc sizes decreased slightly with high air shear stresses owing to the decreased dissolved oxygen. The nitrogen reduction across the membrane via denitrification of the biofilm attached on the membrane surface was also assessed.

Keywords: Membrane bioreactor; COD/N ratio; Biological nutrient removal; Simultaneous nitrification and denitrification; Membrane fouling

1. Introduction

The water environment has been significantly affected by eutrophication, receiving much attention from the research community [1–3]. Nitrogen and phosphorus are the main contributors to this process. The influent concentration of carbon source plays an important role in the simultaneous nitrogen and phosphorus removal process. In the biological nitrogen removal process, nitrifiers conduct anti-nitrification under aerobic condition, and denitrifiers require electron donors to conduct denitrification under anoxic condition. In the biological phosphorus removal process, polyphosphate-accumulating organisms (PAOs) require volatile fatty acids to synthesize poly-β-hydroxybutyrate (PHB) and release phosphorus under the anaerobic conditions, and then the PHB is consumed to obtain energy to increase uptake of phosphorus under aerobic conditions. Natural competition of carbon sources will occur between PAOs and denitrifiers in a simultaneous nitrogen

* Corresponding author.

and phosphorus removal process, especially in an anaerobic reactor [4]. Thus, achievement of an appropriate composition of influent nutrients is a key factor to achieve effective biological nutrient removal (BNR) performance.

Membrane coupling with an activated sludge process is a promising technology with excellent effluent quality, sufficient to meet the standard of municipal and industrial wastewater reclamation [5–8]. Different configurations of membrane bioreactors (MBRs) have been developed for BNR from wastewater (e.g., simultaneous nitrification and denitrification-membrane bioreactor [SND-MBR], anoxic/oxic-membrane bioreactor [A/O-MBR], and enhanced biological phosphorus removal-membrane bioreactor [EBPR-MBR]). Fouling behaviors associated with different configurations of biological nutrient removal-membrane bioreactor (BNR-MBR) processes exhibit different characteristics [9–11]. All parameters involved in the design and operation of MBR processes influence on membrane fouling. Thus, three categories of factors are defined, that is, membrane characteristics, operating conditions, and feed-biomass parameters [12]. Chen et al. [13] quantified interfacial interactions between a randomly rough membrane surface and foulant particles and revealed that the membrane surface characteristics had significant impacts on membrane fouling. The operating conditions (e.g., flux, aeration, crossflow velocity [CFV], and sludge retention time [SRT]) also exhibit substantial influences on membrane fouling, within which some operating parameters can simultaneously affect the biomass characteristics [12]. The biomass quality parameters (e.g., floc size, floc roughness, bound extracellular polymeric substance [EPS], and soluble microbial product [SMP]) have more direct effects on membrane fouling [14,15]. Shen et al. [16] reported a decrease in floc size would greatly increase both of hydraulic cake resistance and osmotic pressure-induced resistance. Bound EPSs and SMPs are considered two main components that affect the biofouling potential of the mixed liquor (ML). Bound EPSs attached on the surface of biofloc is composed of high-macromolecular polyelectrolytes (e.g., protein, carbohydrate, humic compounds, and nucleic acids) and determines the biofloc structure and settling ability, thus affecting the biocake fouling resistance. SMPs are soluble (sol) EPS and are associated with metabolic and biomass decay. SMPs are considered the main contributor to deep pore-blocking resistance, which leads to irreversible fouling due to membrane rejection. Additionally, the gelation of SMP and the colloidal in the presence of calcium ions induce the formation of gel layer, which increases the fouling resistance in MBR processes [17,18].

Different kinds and concentrations of carbon resources also affect the metabolic characteristics of activated sludge and can influence the sustainable filtration process [19–21]. The chemical oxygen demand (COD)/total nitrogen (TN) (COD/N) ratio plays an important role in affecting the quantity and composition of microbial metabolic productions. There is also an effect of influent composition on membrane fouling, as well as an effect of BNR performance. However, few studies have been conducted on the influence of the COD/N ratio on membrane fouling, particularly for a membrane-based BNR process.

In this study, the influences of COD/N ratio on the BNR performance and membrane fouling were comprehensively investigated, using feed wastewater with different carbon concentrations. Physiochemical characteristics and metabolic production of aerobic biosolids under different COD/N ratios were monitored to determine their relationships with biofouling propensity. More specifically, biofloc size distributions and the quantities and compositions of SMP and EPS were determined to analyze the biofouling mechanisms. Modified fouling index (MFI) values of the sol and suspended solid (SS) fractions of the ML were determined to assess membrane fouling propensity under different COD/N ratios. The relationships between nitrogen loss in the aerobic tank and the fouling rate were determined.

2. Materials and methods

2.1. Experimental setup and operation

The bench-scale plant (Fig. 1) is comprised of a bioreactor (total volume 28 L) with a University of Cape Town (UCT)-type configuration (i.e., anaerobic [20% of the total volume], anoxic-1 [20%], and anoxic-2 [20%] reactor compartments, followed by a compartment [40%] with a submerged flat sheet membrane [pore size, 0.4 μm; surface area, 0.1 m^2; made of chlorinated polyethylene of Kubota Corporation, Japan]). The anaerobic and anoxic reactor compartments each include a mixer. An online pH-dissolved oxygen (DO) sensor (WTW Multi 340i) is installed in the aerobic membrane reactor compartment. The bench-scale University of Cape Town-membrane bioreactor (UCT-MBR) process is controlled with a programmable logic controller and data acquisition system that controls all the automatic control loops of the plant. Constant flux (20 $L{\cdot}h{\cdot}m^{-2}$) and intermittent suction (9 min suction and 1 min rest) were utilized during the experiment. Feed synthetic wastewater from the storage tank is pumped to the anaerobic reactor followed by anoxic tank-1, anoxic tank-2, and then the aerobic-membrane tank, and finally pumped out through the membrane module. The temperature can be controlled by a heater that is submerged in anoxic tank-1. The operational parameters are listed in Table 1.

2.2. Synthetic municipal wastewater and seed sludge

The UCT-MBR plant was fed with synthetic municipal sewage water (real municipal sewage mixed with an acetate and ammonia chloride solution to a set the influent COD/N ratio) and the seed sludge was taken from the east wastewater treatment plant of Handan, Hebei Province, which employs a *T*-type oxidized ditch process, achieving satisfactory biological nitrogen removal. The pH was controlled at 7.2–7.4 by the addition of NaOH and HCl solution. Temperature was controlled at 20°C–23°C using a heater. The major characteristics of the influent under different operational periods are shown in Table 2. After 2-month cultivation, stable performance of biological nitrogen and phosphorus removal was achieved in the UCT-MBR process.

2.3. Membrane resistance determination

The trans-membrane pressure (TMP, kPa) data were calibrated by the standard temperature (*T*, 20°C) using Eq. (1) [22].

$$TMP = TMP_{T} \cdot e^{0.0239 \cdot (T-20)} \quad (1)$$

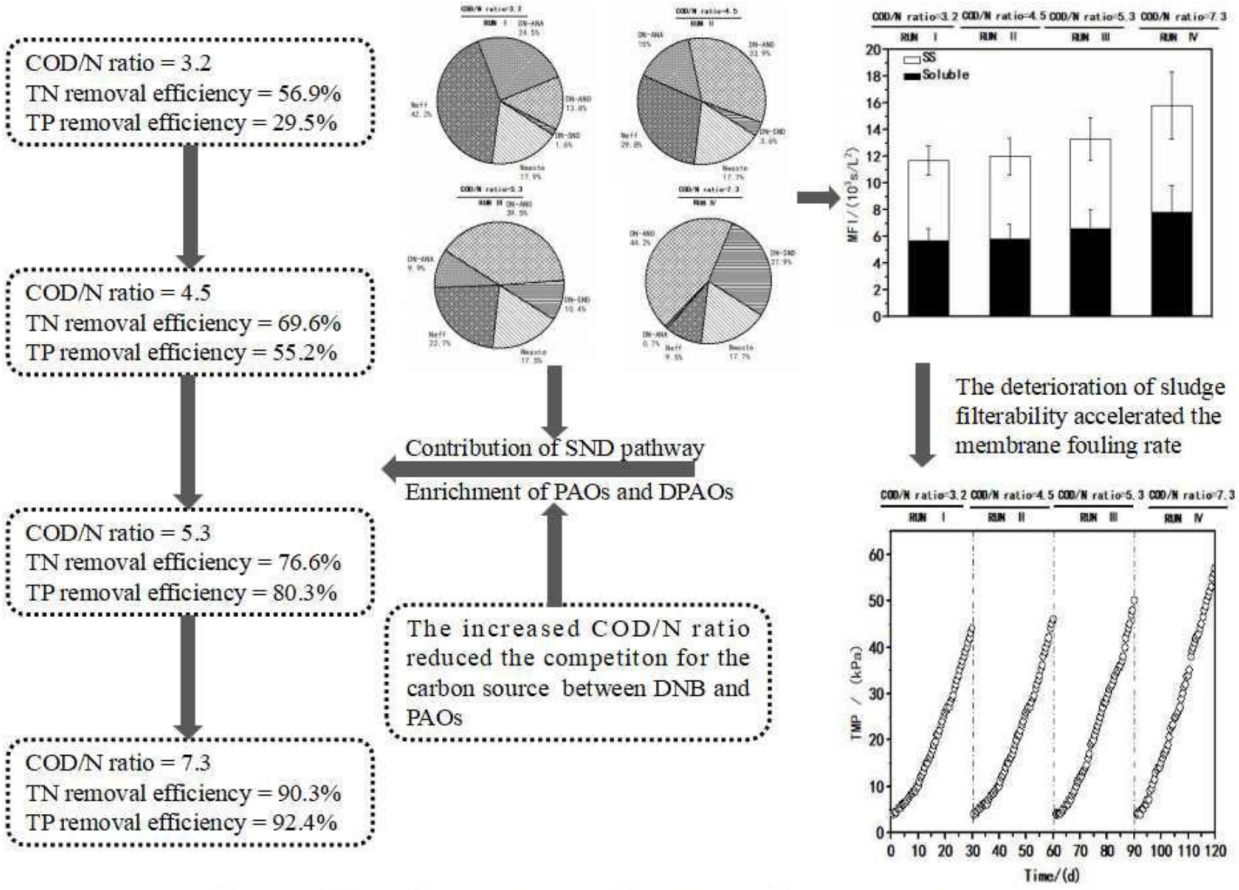

The effect of influent COD/N ratio on UCT-MBR process treating wastewater

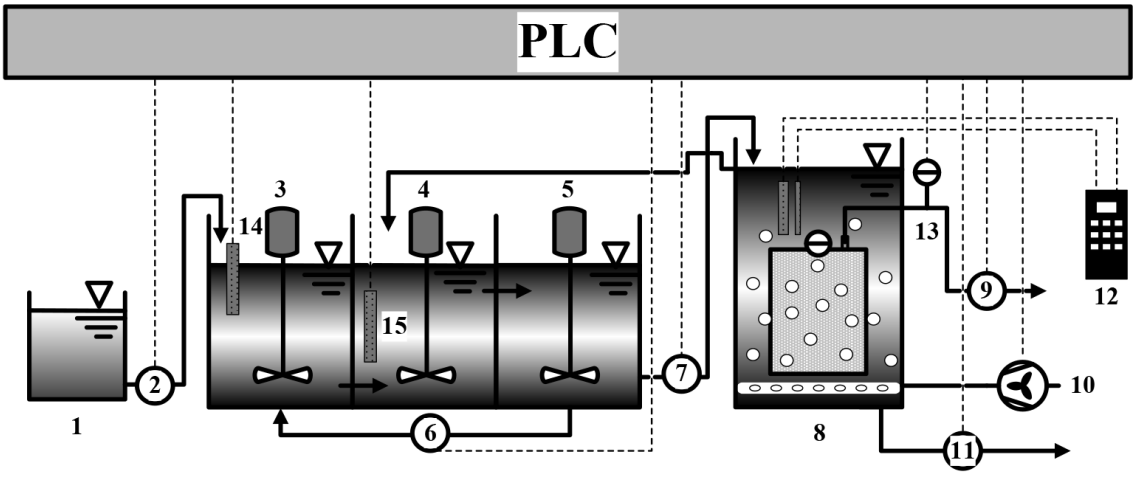

1 storage tank; 2 influent pump; 3 anaerobic tank; 4 anoxic tank-1; 5 anoxic tank-2; 6 recycling pump; 7 sludge lift pump; 8 aerobic membrane tank; 9 permeate pump; 10 air compressor; 11 sludge discharge pump; 12 DO/pH sensor; 13 pressure gauge; 14 water level controller; 15 heater

Fig. 1. Schematic diagram of the UCT-MBR process.

Membrane resistance was analyzed based on Darcy' law, as shown in Eq. (2) [23].

$$J=\frac{\mathrm{TMP}}{\mu R_t}=\frac{\mathrm{TMP}}{\mu(R_f+R_m)}=\frac{\mathrm{TMP}}{\mu(R_c+R_p+R_m)} \quad (2)$$

where R_t is the total hydraulic resistance, R_m is the membrane resistance, R_c is the cake layer resistance, R_p is the pore blocking resistance, μ is the dynamic viscosity of the permeate, and J is the membrane permeate flux. Each resistance was determined according to the following experimental procedures: R_m was computed by measuring the flux and TMP of tap water using a new flat sheet membrane, R_t was evaluated from the final data after biomass microfiltration, the cake layer on the membrane surface was wiped with a sponge and simultaneously flushed by tap water, and the membrane was then submerged in tap water to obtain flux and TMP data to calculate $R_m + R_p$. Then R_c and R_p were determined by subtraction according to Eq. (2). A new flat sheet membrane was used for each month-long operation cycle.

The fouling rate (F_r, kPa/h) was determined based on the increase of TMP for the same period of time, as shown in Eq. (3) [24].

$$F_r=\frac{\mathrm{dTMP}}{\mathrm{d}t}=\frac{\mathrm{TMP}_{\mathrm{end}}-\mathrm{TMP}_{\mathrm{initial}}}{t_{\mathrm{end}}-t_{\mathrm{initial}}} \quad (3)$$

2.4. Chemical and physical analytical methods

COD, sol COD (sCOD), NH_4^+-N, NO_2^--N, NO_3^--N, TN, TP, mixed liquor suspended solid (MLSS), and mixed liquor volatile suspended solid (MLVSS) were measured according to standard methods [25]. The sludge samples were obtained from the aerobic membrane tank at the end of each run and used to measure biofloc size and the amounts of bound EPS and SMP. The biofloc size distribution was determined by a Malvern Mastersizer 2000 instrument (Worcestershire, UK) with a detection range of 0.02–2,000 mm. The scattered light was detected by means of a detector that converts the signal to a size distribution based on volume. Each sample was measured three times with a standard deviation of 0.1%–1.5%.

Table 1
Operational parameters

Parameters	Values
Total hydraulic retention time, h	15.5
SRT, d	20–25
ANO2-ANA recirculation (r_1), % of inflow	400%
AER-ANO1 recirculation (r_2), % of inflow	100%
Aeration rate, L·h^{-1}	100
Temperature, °C	21–23

2.5. Sample extraction and fractionation

Two parallel sludge mixture samples were removed and immediately cooled to 4°C to minimize microbial activity. Each sludge mixture was centrifuged for 15 min at 12,000 g to remove the SSs, and the protein and carbohydrate concentrations of the supernatant after membrane microfiltration with pore size 0.45 μm were determined and represent the SMP. The bound EPS concentration was measured as the amount of carbohydrate and protein using a cation exchange resin (CER) (Dowex Marathon C, Na^+ from, Sigma-Aldrich, USA) extraction method [26]. Sludge collected from the aeration tank was centrifuged at 12,000 g for 15 min. The supernatant was discarded and the sludge was re-suspended in the same amount of buffer solution. The buffer solution consisted of 2 mM Na_3PO_4, 4 mM Na_2HPO_4, 9 mM NaCl, and 1 mM KCl. CER (75 g of CER/gVSS) was added to each sludge and mixed at 800 rpm for 2 h at 4°C, and then the mixture was centrifuged at 12,000 g for 15 min. The supernatant was microfiltered through the membrane with pore size of 0.45 μm, and the filtered sample represented the total amount of bound EPS. The total protein content was determined using the modified Bradford method. Bovine serum albumin was used as a protein standard and the total carbohydrate content was determined using the anthrone-sulfuric acid colorimetric method with glucose as the standard.

2.6. Batch filtration tests

MFI was determined to compare the biofouling characteristics in terms of bound EPS and SMP. Batch filtration tests were conducted by using a stirred batch cell (8200, Amicon, USA) to measure the permeate volume with an ultrafiltration (UF) membrane (nominal molecular weight limit 300 kDa, polyethersulfone, 28.7 cm^2, Millipore Corp., USA), under constant pressure (30 kPa). Two samples were applied

Table 2
Operational periods of the experiment

Operational stages	RUN I (1–30 d)	RUN II (31–60 d)	RUN III (61–90 d)	RUN IV (91–120 d)
COD (mg/L)	156.8	222.3	267.3	360.5
F_{COD}/M (gCOD/gMLSS·d^{-1})	0.062	0.088	0.11	0.14
TN (mg/L)	48.8	49.3	50.1	49.5
COD/N ratio	3.2/1	4.5/1	5.3/1	7.3/1
F_{TN}/M (gTN/gMLSS·d^{-1})	0.019	0.02	0.02	0.02
TP (mg/L)	6.1	5.9	5.8	6.2
COD/P ratio	25.7/1	37.7/1	46.1/1	58.1/1
F_{TP}/M (gTP/gMLSS·d^{-1})	0.002	0.002	0.002	0.002

to fractionate the membrane foulants into sol and SS components. First, the sludge mixture from aerobic membrane reactor containing the sol and SS components was filtered through UF membranes in the stirred batch cell (Fig. 2). Second, the sol component (obtained by the same procedure as described for SMP) of the sludge mixture was filtered through UF membranes in the stirred batch cell. A plot of t/V versus V (t in s and V in L) was then constructed to determine the MFI according to Eqs. (4) and (5) [27]. The SS component was calculated by subtraction of the sol component from the sludge mixture.

$$\frac{t}{V}=\frac{\mu R_m}{\Delta P}+\frac{\mu\alpha C}{2\Delta P}V \tag{4}$$

$$\text{MFI}=\frac{\mu\alpha C}{2\Delta P} \tag{5}$$

2.7. Calculation of nitrogen removal via SND in the UCT-MBR

Based on the nitrogen balance, the nitrogen removal via different pathways was calculated specifically using the Eqs. (6)–(8) [3].

$$\text{DN}_{\text{SND}}=\text{N}_{\text{inf}}-\text{N}_{\text{eff}}-\text{N}_{\text{assimilation}}-\text{DN}_{\text{ANA}}-\text{DN}_{\text{ANO}} \tag{6}$$

$$\text{DN}_{\text{SND}}=\text{DN}_{\text{mem}}+\text{DN}_{\text{AER}} \tag{7}$$

$$\text{N}_{\text{assimilation}}=\text{MLSS}_{\text{waste}}\times f_{\text{vss/ss}}\times V_{\text{waste}}\times f_{\text{N/biomass}} \tag{8}$$

where N_{INF} and N_{eff} are the influent and effluent nitrogen amount, respectively, gN/d; N_{waste}, DN_{ANA}, DN_{ANO}, and N_{SND} represent the nitrogen removed via cell assimilation, pre-denitrification in the anaerobic tank, pre-denitrification in anoxic tank-1 and tank-2, and SND in the aerobic membrane tank, respectively, gN/d; DN_{mem}, and DN_{AER} represent the nitrogen removed via SND on the membrane surface and in the ML, respectively, gN/d; V_{waste} is the waste sludge daily discharge amount, L; and $f_{\text{N/biomass}}$ represents the nitrogen ratio of the total biomass, 12.39% [28].

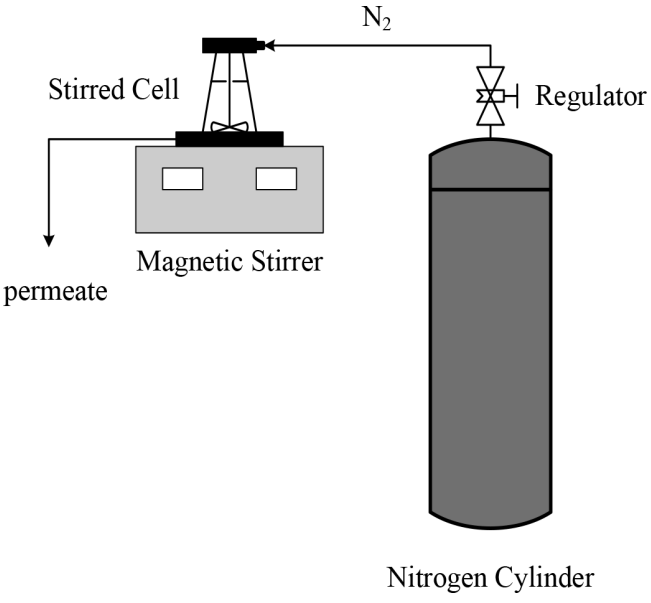

Fig. 2. Schematic diagram of the stirred batch cell system.

2.8. Calculation of anaerobic phosphorus release and anoxic phosphorus removal efficiency

Based on the phosphorus balance, the anaerobic phosphorus release (P_{ANA}, mg/L) and the anoxic phosphorus removal efficiency (T, %) were calculated using Eqs. (9) and (10) [29].

$$P_{\text{ana}}=c_{\text{ana}}-\frac{c_{\text{ano2}}r_2+c_{\text{inf}}}{1+r_2} \tag{9}$$

$$T=1-\frac{(1+r_1+r_2)c_{\text{ano2}}}{(1+r_2)c_{\text{ana}}+r_1c_{\text{aer}}} \tag{10}$$

where C_{INF} refers to the phosphate concentration in the influent; C_{ANA}, C_{ANO2}, and C_{AER} refer to the effluent phosphate concentrations in the anaerobic, anoxic tank-2, and aerobic membrane tanks, respectively, mg/L; and r_1 and r_2 refer to the recycle from the aerobic tank to the anoxic tank-1 and from the anoxic tank-2 to the anaerobic tank, respectively, %.

3. Results and discussion

3.1. The Effect of COD/N ratio on overall BNR performance

3.1.1. COD removal

There were different COD concentrations in the influent, supernatant, and effluent under different COD/N ratios throughout operation as shown in Fig. 3. On average, 86.2% of COD was removed for a COD/N ratio of 3.2. During the next three runs, the removal efficiencies of COD were 89.4%, 90.9%, and 93%, with effluent of 23.6, 24.2, and 25.1 mg/L

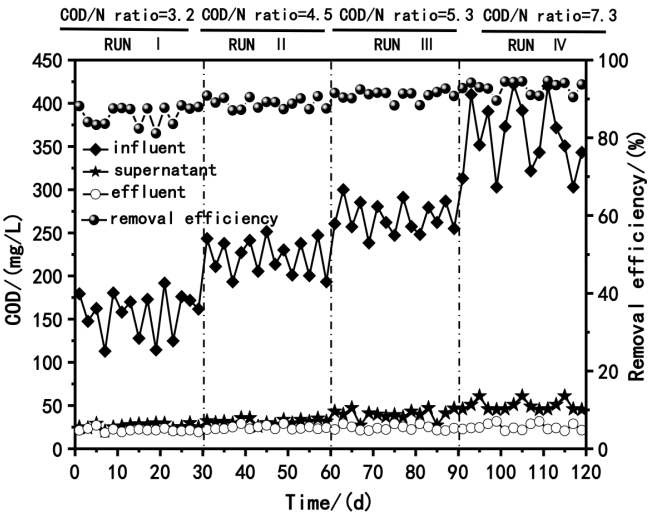

Fig. 3. Performance of COD removal during operational periods.

under COD/N ratio of 4.5, 5.3, and 7.3, respectively. COD removal efficiencies were independent of COD/N ratios based on the high organic matter removal data. As shown in Fig. 4, the volume loading removal increased with influent volume loading, indicating that the UCT-MBR has a strong capability of anti-shocking loading. However, it should be noted that the process still operated under the low-organic loading condition (ranging from 0.25 to 0.58 g COD/L·d, obviously lower than that of the typical anaerobic condition). Many previous studies have shown consistent high COD removal efficiency in the MBR process was due to the high MLSSs and membrane rejection [30].

3.1.2. Nitrogen removal

Throughout operation, the removal efficiency of NH_4^+-N remained above 99%, with good COD removal performance irrespective of COD/N ratios, as shown in Fig. 5. In contrast, TN removal performance was more affected by influent COD/N ratios because electronic donors were needed during the denitrification process. During RUN I (COD/N ratio of 3.2), the NH_4^+-N and TN concentrations in the effluent were

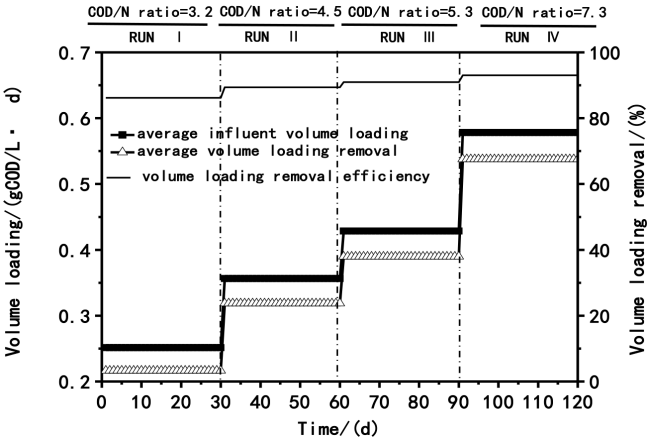

Fig. 4. Changes of volume loading removal with variations of influent volume loading.

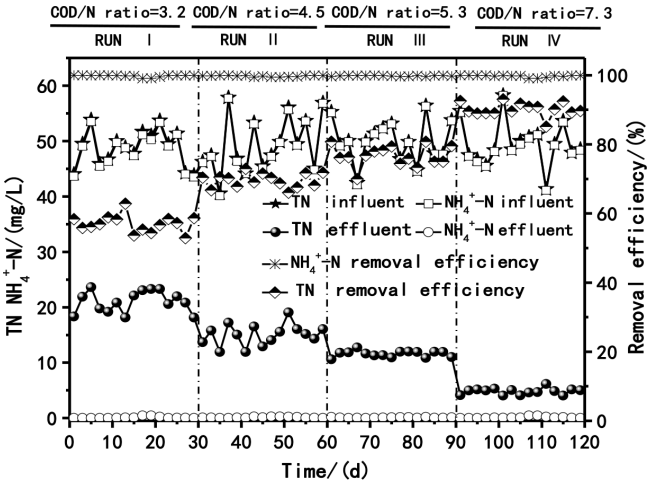

Fig. 5. Nitrification and denitrification in the UCT-MBR process during operational periods.

0.1 and 21 mg/L on average, with removal efficiency of 99.8% and 56.9%, respectively. The deteriorated TN removal performance was attributed to the influent-limited carbon source. At a COD/N ratio of 7.3 (RUN IV), nearly complete nitrification was achieved despite the increased influent organic volume loading, with an average removal efficiency of 99.8%. Nitrification activity was not affected by the COD/N ratio, mainly due to longer SRT and the membrane rejection of nitrifiers. At the same time, the removal efficiency of TN was 90.3%, with an average NO_3^--N concentration of 4.7 mg/L in the effluent. The nitrogen removal performance exhibited an increasing trend with influent COD/N ratio as shown in Fig. 6. Higher influent COD/N ratio and higher TN removal efficiency were obtained during operation. For an influent COD/N ratio of 5.4, greater than 77% removal efficiency of TN was achieved.

3.1.3. Nitrogen removal pathway under varying COD/N ratios

The changes in the nitrogen removal pathway under different COD/N ratios are shown in Fig. 7. DO is considered a key factor affecting the SND process. NO_X^--N can be utilized as the electronic acceptor by denitrifiers if organic carbon is needed under anoxic conditions. Contributions of SND to TN removal increased with increasing COD/N ratio in the influent. At a COD/N ratio of 3.2, the amounts of nitrogen removal via pre-denitrification in the anoxic and anaerobic tanks were 13.8% and 24.5% with a DO concentration of 3.1 mg/L in the aerobic tank. During RUN III and RUN IV, 10.54% and 27.9% of the amount of influent nitrogen were removed via SND at a DO concentration of 1.4 and 0.9 mg/L, respectively. Higher TN removal efficiency was achieved due to the contribution of the SND process, which was induced by the decreased DO concentration due to the increased COD/N ratio.

3.1.4. Phosphorus removal

Total phosphorus (TP) removal performance under different COD/N ratios was measured in Fig. 8. The TP removal

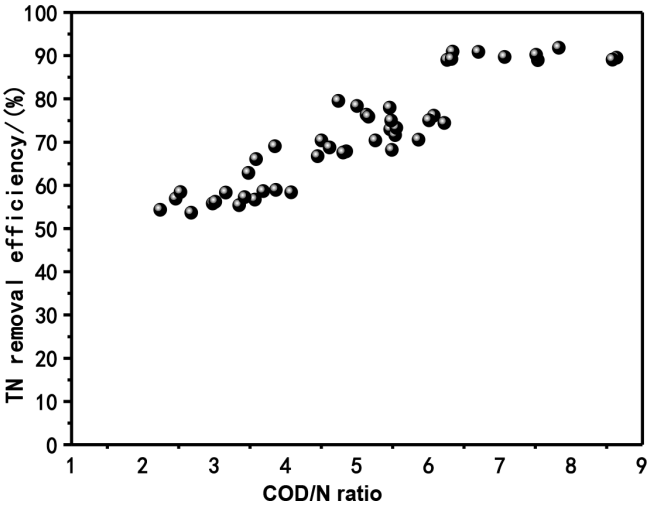

Fig. 6. Changes of TN removal efficiency with variations of COD/N ratio.

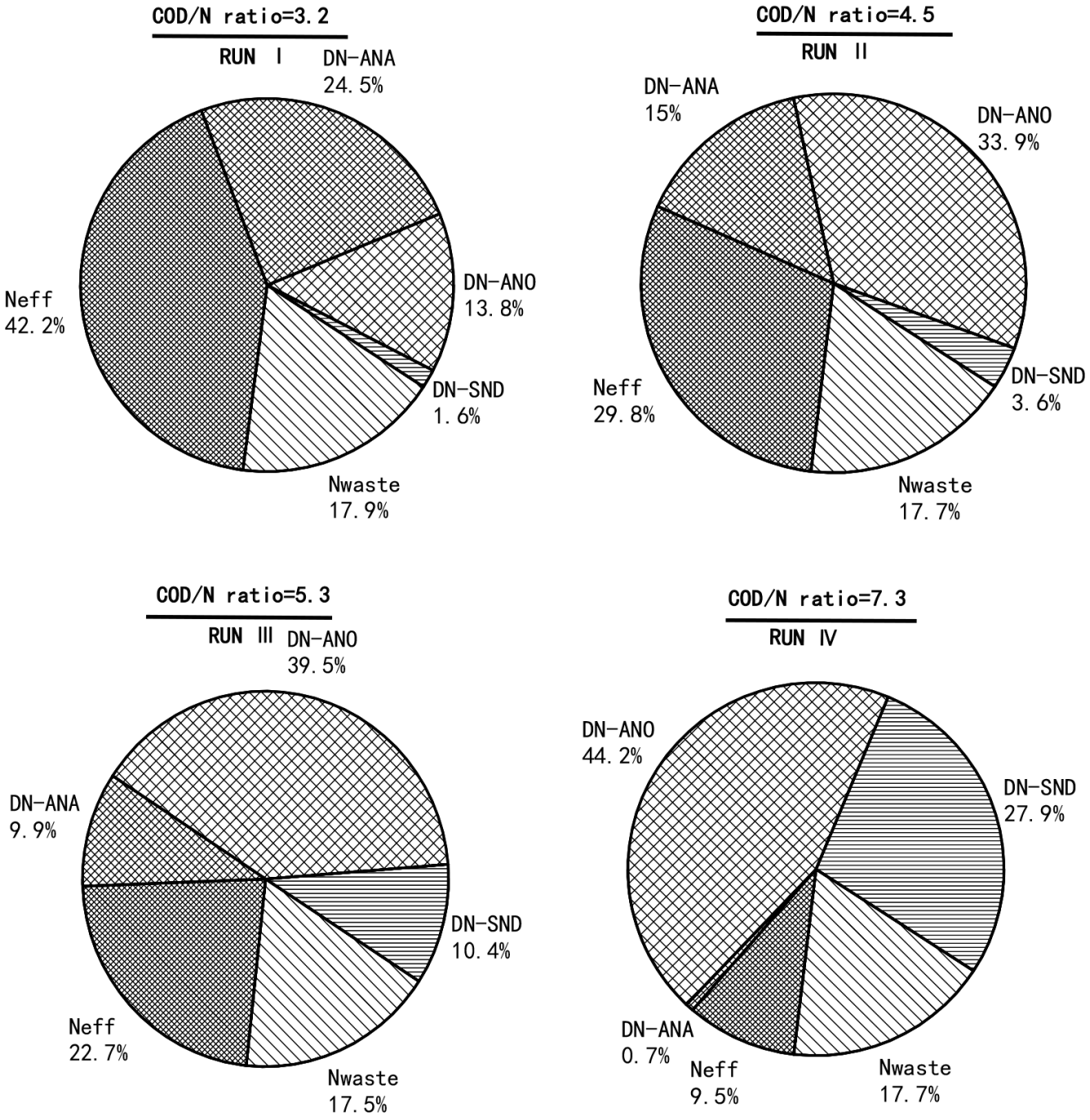

Fig. 7. Changes in the nitrogen removal pathway during operational periods.

efficiency was only 29.5% at a COD/N ratio of 3.2. High concentrations of NO_3^--N from anoxic tank-2 influenced the phosphorus released due to carbon-source competitions between the polyphosphate-accumulating organisms (PAOs) and denitrifiers in the anaerobic tank. PAOs could not release phosphorus effectively, due to the insufficient carbon source available to change into PHB. In the aerobic condition, the energy needed for excessive phosphorus uptake could not be accessed because there was an insufficient amount of PHB present in the anaerobic condition. The amount of phosphorus released in the anaerobic tank increased as the influent COD/N ratio increased. In addition to the material utilized by the denitrifiers, PAOs could uptake the remaining carbon source to change into PHB. As shown in Table 3, the phosphorus released by PAOs was 46.82 mg/L at a COD/N ratio of 7.4, almost twice the phosphorus concentration at a COD/N ratio of 5.4.

It was obvious that anoxic phosphorus uptake occurred, because there was a decrease of phosphorus from anoxic-1 to anoxic tank-2, and anoxic phosphorus uptake was enhanced during operation. The amount of anoxic phosphorus uptake was influenced by the amount of phosphorus released in the

anaerobic tank. The anoxic phosphorus removal efficiencies were 30.87%, 41.21%, and 44.91% for a COD/N ratio of 4.6, 5.4, and 7.4, respectively. The deteriorated phosphorus removal efficiency was not observed in the lower DO condition. When there was pre-denitrification, part of the PAOs in the anoxic tanks was cultivated to have denitrification ability. PHB was used as the electron donor in the denitrification process by denitrifying poly-phosphate accumulating organisms

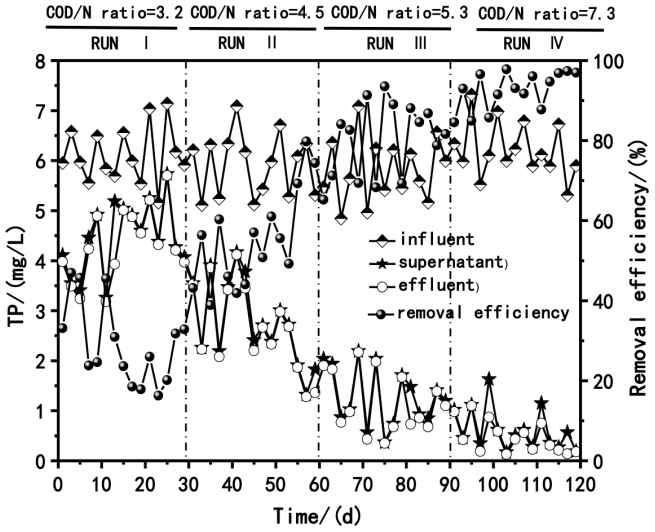

Fig. 8. Performance of phosphorus removal during operational periods.

(DPAOs), with simultaneous uptake of phosphorus under anoxic conditions [31]. The TP removal mainly depended on the biological process, and colloid phosphorus was removed by membrane rejection. Furthermore, as shown in Table 3, phosphorus was mainly removed via the biological process. The increased COD/N ratio in the influent could supply enough electron donors for denitrification bacteria and PAOs to reduce the carbon-source competition. A higher phosphorus removal efficiency was achieved due to the enrichment of DPAOs and PAOs.

Overall, the COD removal efficiency (93.0% at COD/N ratio of 7.4) for municipal wastewater in this process was lower than that (≥95.0%) for industrial waster (e.g., olive mill wastewater) using an anaerobic MBR process due to the lower organic loading in the feed. At the same time, the nitrogen and phosphorus removal efficiencies (90.3% and 92.4% at COD/N ratio of 7.4) were higher than those (~17.5% and ~81.0%) for industrial waster treated using an anaerobic MBR process due to the alternate anaerobic, anoxic and oxic conditions [32,33].

3.2. Membrane fouling characteristics and mechanisms under varying COD/N ratios

3.2.1. Membrane fouling characteristics

Fouling characteristics under different COD/N ratios were measured and are shown in Fig. 9. Higher fouling rates were observed for higher influent COD/N ratios. During RUN IV, TMP_{end} reached 57 kPa with a fouling rate of 0.074 kPa/h,

Table 3
Changes of COD, nitrogen, and phosphorus in bioreactors during operational periods

COD/N DO (mg/L)	Value (mg/L)	INF	ANA	ANO1	ANO2	AER-MEM	EFF
3.2/1	COD	156.8	36.8	26.5	24.7	26.4	21.7
3.1 ± 0.7	NH_4^+-N	48.4	22.1	9.1	8.9	0.13	0.1
	NO_3^--N	0.32	0.81	14.2	13.2	21.1	20.9
	NO_2^--N	0.05	0.02	0.02	0.04	0	0
	TP	6.1	9.5	6.1	5.8	4.7	4.3
4.6/1	COD	222.3	47.4	33.9	32.4	31.5	23.6
2.2 ± 0.6	NH_4^+-N	49.1	23.2	9.5	9.2	0.14	0.12
	NO_3^--N	0.21	0.21	8.8	7.6	15.5	14.9
	NO_2^--N	0.02	0.01	0.01	0.02	0	0
	TP	5.9	19.4	7.09	5.74	2.74	2.67
5.4/1	COD	267.3	48.6	40.6	37.5	39.7	24.2
1.4 ± 0.5	NH_4^+-N	49.9	24.2	9.9	9.4	0.16	0.1
	NO_3^--N	0.13	0.02	5.5	4.9	12.3	11.5
	NO_2^--N	0.02	0.03	0.01	0.02	0	0
	TP	5.8	38.1	9.62	7.94	1.21	1.16
7.4/1	COD	360.5	52.5	45.13	46.5	50.6	25.1
0.9 ± 0.4	NH_4^+-N	49.3	25.2	9.7	8.5	0.13	0.12
	NO_3^--N	0.21	0.02	0.26	0.21	5.81	4.7
	NO_2^--N	0.01	0.03	0.01	0.03	0	0
	TP	6.2	55.1	12.39	10.36	0.67	0.47

Note: INF – Influent; ANA – Anaerobic tank; ANO1 – Anoxic tank-1; ANO2 – Anoxic tank-2; AER-MEM – Aerobic membrane tank; and EFF – Effluent.

almost 32% higher than that measured for RUN I. The distributions of membrane filtration resistances were analyzed to examine the fouling tendencies (Table 4). Bioflocs, colloids, and solutes were deposited on the membrane surface during the filtration process, and the biocake resistance became the dominant resistance, accounting for more than 86% of the total resistance under varying COD/N ratios. For RUN I, the resistances of biocake and deep pore clogging were 52.45 and 1.9 (10^{11} m^{-1}), 89.5% and 3.2%, respectively, of the total. The contributions of biocake resistance to the total resistance decreased due to the increase of deep pore-blocking resistance, although the actual biocake resistance also increased.

The structural characteristics of the new membrane, biocake layer, and deep pores are shown in Fig. 10. Clear pores were distributed uniformly in the new membrane. After RUN III, biocake was formed densely on the surface of the membrane and filled almost all the membrane pores. It was also observed that (Fig. 10(c)) that deep pores were blocked by the deposition and adsorption of colloids and solutes, resulting in irreversible fouling.

3.2.2. Hydraulic resistance of ML

The nitrogen removal pathway under varying COD/N ratios was discussed in section 3.1.3. The SND behavior can account for the changes of physiochemical properties of the ML, which then influence the fouling characteristics under different COD/N ratios. The hydraulic resistance attributed to the individual fraction of the ML was determined in the batch filtration experiment. Despite the different filtration conditions of constant flux mode in the flat sheet MBR versus constant pressure mode in the MFI test, there was an increasing trend with total MFI in the reactor under varying COD/N ratio, as shown in Fig. 11. The MFI values for the sol, SS, and ML, under varying COD/N ratios were measured and are presented in Fig. 12. For RUN I, the SS MFI accounted for ~51% of the ML resistance and the sol MFI accounted for ~ 49% of the ML resistance for both MBRs. For RUN IV, the SS, sol, and total MFI were 7.8, 8, and 15.8 s/L^2, values that are 36.8%, 33.3%, and 35% higher than that measured for RUN I, which can explain the observed higher fouling rates.

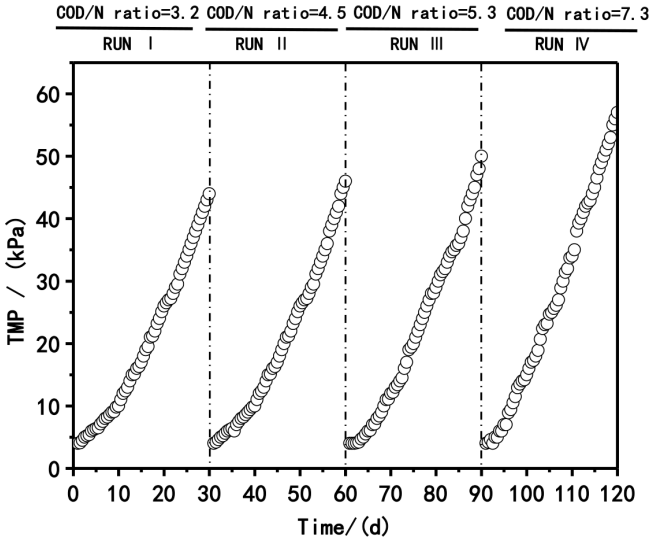

Fig. 9. Changes of TMP in the UCT-MBR process during operational periods.

3.2.3. Bound EPS

Table 5 shows the quality and composition of bound EPS in the aerobic tank for different COD/N ratios. Carbohydrates and proteins are usually the major constituents of the bound EPS. The amount of bound EPS increased as the COD/N ratio increased, and carbohydrate was the main fouling component. In contrast, the ratio of carbohydrate to protein decreased (ranging from 4.5 to 3) as the COD/N ratio increased, indicating that protein-like substances played an increasing importantly role in the biocake structure. More specifically, the carbohydrate and protein of bound EPS were 8.5 and 1.9 mg/gMLVSS, respectively, for RUN I. In RUN IV, where there was obvious SND in the aerobic tank, the carbohydrate and protein of bound EPS increased by 31.8% and 94.7% compared with the levels measured in RUN I. This can also explain the higher SS resistance, because there were higher bound EPS levels observed with higher SND, and increased bound EPS concentration resulted in an increase amount of bound EPS attached to the membrane surface, consistent with findings of other studies [27].

3.2.4. SMP

The concentration and composition of SMP during operation in terms of carbohydrate and protein were measured and listed in Table 6. The sCOD of the supernatant in the membrane tank was used as the SMP indicator. The differences in SMP concentration and composition under different COD/N ratios confirmed that microbial metabolic production differed with changes in the nitrogen removal pathway. The total concentration of sCOD remained around 20.5 mg/L, with carbohydrate of 8.9 mg/L and protein of 1.2 mg/L for RUN I. The total sCOD concentration in terms of carbohydrate and protein increased as the COD/N ratio increased. The concentrations of sCOD, carbohydrate, and protein

Table 4
Membrane filtration resistance during operational periods

Operational periods	Items (%)				
	TMP_{end}	R_c (10^{11} m^{-1})	R_p (10^{11} m^{-1})	R_m (10^{11} m^{-1})	R_t (10^{11} m^{-1})
RUN I	44 kPa	52.45 (89.5)	1.9 (3.2)	4.25 (7.3)	58.6
RUN II	46 kPa	54.35 (88.6)	2.7 (4.5)	4.25 (6.9)	61.3
RUN III	50 kPa	59.65 (88.6)	3.1 (4.7)	4.25 (6.3)	67
RUN IV	57 kPa	65.7 (86.7)	5.95 (7.7)	4.25 (5.6)	75.9

that were measured for RUN I were twice as high as those observed for RUN IV, resulting in higher fouling rates.

The permeate concentrations for SMP for RUN I were examined as shown in Table 6. For RUN I, the rejection percent of carbohydrate, protein, and sCOD were 24.7%, 41.7%, and 25.8%, and the corresponding values for RUN II were 28.3%, 40%, and 33.6%, respectively. Although there were fluctuations of the rejection percentages of carbohydrate (from 24.7% to 33.4%) and protein (from 38.9% to 58.1%) from RUN I to RUN IV, the sCOD rejection percentage increased with increasing COD/N ratios, indicating that the higher SMP rejection under the SND state relative to the higher DO condition was due to the higher retention of SMP under SND state and the increased membrane-fouling rate, as confirmed by higher sol MFI values.

3.2.5. Biofloc size distribution

Biofloc size distributions in the aerobic membrane tank under varying COD/N ratios were measured, as shown in Fig. 13 and Table 7. Previous research showed that biocake fouling resistance was significantly altered by the biofloc size and was also affected by the complex background of the sludge mixture (i.e., aeration shear stress and DO). Constant

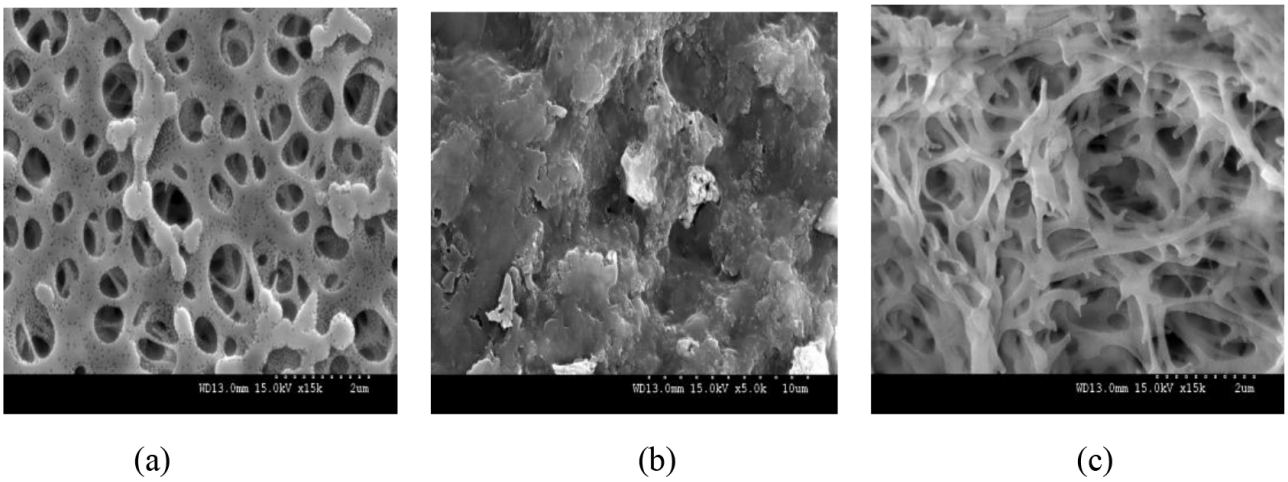

Fig. 10. The scanning electron microscope photographs of (a) new membrane; (2) biocake layer; and (3) deep pores after RUN III.

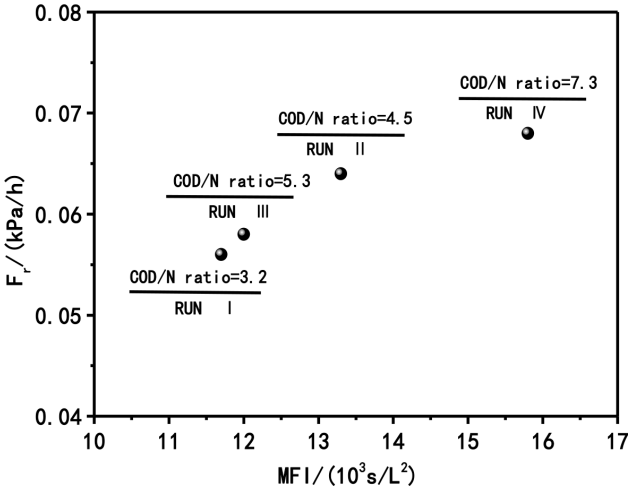

Fig. 11. Changes of membrane-fouling rate with variations of MFI of the mixed liquor in the aerobic membrane tank.

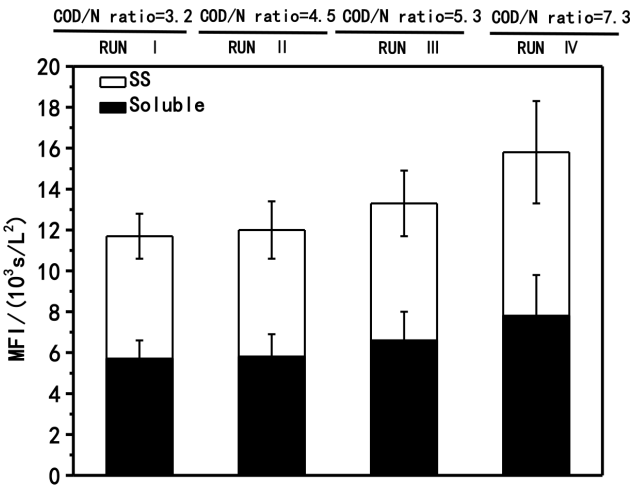

Fig. 12. Filterability of activated sludge in the aerobic membrane tank during operational periods.

Table 5
Quality and composition of bound EPS in the aerobic membrane tank during operational periods

COD/N	Bound EPS (mg/gMLVSS)	Carbohydrate (mg/gMLVSS)	Protein (mg/gMLVSS)	Carbohydrate/protein
Run I	10.5 (±2.3)	8.5 (±1.4)	1.9 (±0.8)	4.5
Run II	11.6 (±2.5)	9 (±1.9)	2.4 (±1)	3.8
Run III	12.6 (±3.1)	9.8 (±2.1)	2.8 (±1.1)	3.5
Run IV	14.9 (±3.6)	11.2 (±2.9)	3.7 (±1.4)	3

aeration intensity was maintained during the whole operation and the same CFV was obtained for the same shear stress. Slight differences in the biofloc sizes were induced by the changes of DO, which were significantly affected by influent organic loading. The biofloc size decreased from 53.975 to 49.287 μm as the DO decreased from 3.1 to 0.9 mg/L. A lowering of cell surface hydrophobicity under the oxygen-limited state could disrupt the flocculation ability of microbial aggregates. The biofloc size became smaller under limited oxygen and decreased settling was observed with bulking [34]. In contrast, Arabi and Nakhla [27] reported that larger biofloc sizes were found in the SND-MBR compared with those in the aerobic-MBR. In this experiment, aeration intensity was controlled for a lower DO state, so there was lower aeration shear stress in the SND-MBR than in the aerobic-MBR.

3.2.6. Changes of membrane fouling with denitrification

Nitrogen loss across the membrane was calculated as the NO_3^--N reduction. The effect of DO and sCOD on NO_3^--N reduction was evaluated as shown in Fig. 14. A reduction in the sCOD reduction in the range of 5.3–22.2 mg/L was observed in the SMP rejection with NO_3^--N reduction ranging from 0.2 to 1.11 mg/L. It has been reported that denitrification can be conducted by biofilm on the membrane surface [35], reducing membrane permeability. Matějů et al. [36] calculated that 4.2 gCOD/g N was needed for denitrification considering biomass formation, but the observed sCOD reduction was higher than the theoretical amount, confirming that other parts of sCOD were rejected by the accumulation of biocake layer in the membrane tank. It can be clearly seen from the data presented in Fig. 14 that the concentration of sCOD and NO_3^--N reduction decreased as DO increased, indicating that DO acted as a key factor of SND occurrence in the biofilm attached on the membrane surface.

The changes of the membrane-fouling rate with variations of nitrogen removal via SND in the aerobic membrane tank are shown in Fig. 15. An increased fouling rate was observed with the increase of DN_{mem}, DN_{AER}, and DN_{SND}, indicating that SND in the membrane tank was the major factor contributing to a higher fouling rate, which may suggest the COD/N ratio directly influenced DO.

Table 6
SMP concentration and composition and permeates and SMP rejections in the aerobic membrane tank during operational periods

Run periods	Items (mg/L)	MBR tank	Permeate	Rejections
Run I	SMP_C	8.9 (±2.1)	6.7 (±1.8)	24.7%
	SMP_P	1.2 (±0.6)	0.7 (±0.3)	41.7%
	sCOD	20.5 (±3.2)	15.2 (±2.9)	25.8%
Run II	SMP_C	11.3 (±2.8)	8.1 (±1.8)	28.3%
	SMP_P	1.5 (±0.8)	0.9 (±0.2)	40%
	sCOD	26.2 (±3.5)	17.4 (±3.4)	33.6%
Run III	SMP_C	16.3 (±6.2)	12.1 (±4.1)	25.8%
	SMP_P	1.8 (±0.6)	1.1 (±0.4)	38.9%
	sCOD	33.6 (±4.3)	19.8 (±3.2)	41.1%
Run IV	SMP_C	25.3 (±4.8)	16.6 (±3.7)	34.4%
	SMP_P	3.1 (±1.2)	1.3 (±0.7)	58.1%
	sCOD	43.3 (±6.1)	21.1 (±4.3)	51.3%

4. Conclusion

Nutrient removal performance of the UCT-MBR was highly influenced by COD/N ratios. A high COD/N ratio (7.3) can alleviate the consequences of natural competition for carbon among denitrifiers and PAOs, and the anoxic phosphorus process was enhanced to account for 44.93% of TP removal

Table 7
Biofloc size distribution in the aerobic membrane tank during operational periods

Operational periods	d (0.1) (μm)	d (0.5) (μm)	d (0.9) (μm)	Standard deviation
RUN I	22.643	53.975	104.754	0.422%
RUN II	21.009	52.883	101.817	0.610%
RUN III	21.676	50.923	103.521	0.611%
RUN IV	22.041	49.287	95.243	0.759%

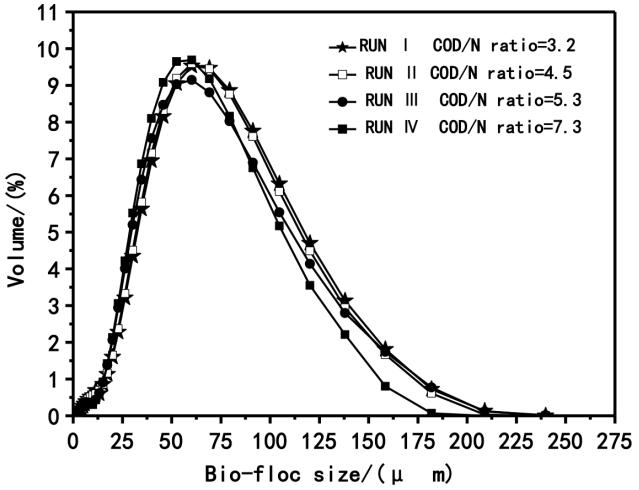

Fig. 13. Changes of biofloc size in the aerobic membrane tank during operational periods.

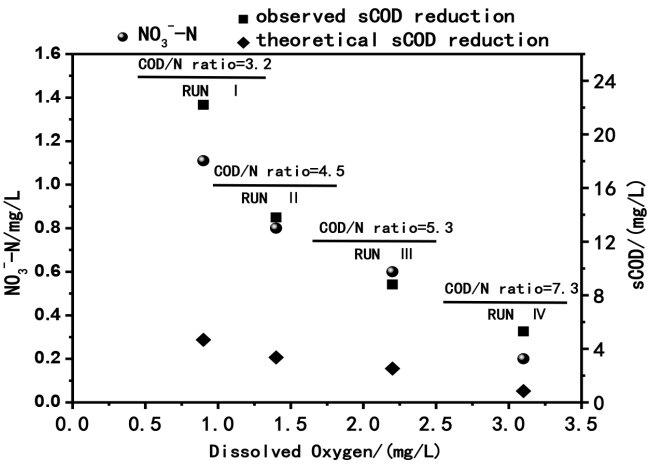

Fig. 14. Denitrification on membrane surface associated with DO and sCOD.

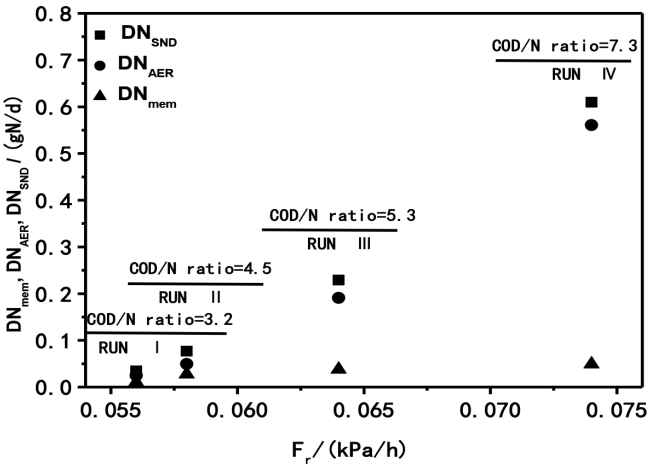

Fig. 15. Changes of membrane-fouling rate with variations of the nitrogen loss in the aerobic membrane tank.

by DPAOs. Contributions of TN removal via aerobic SND increased to 27.9% from 1.6% (COD/N ratio of 3.2) because an increasing COD/N ratio changes the pathways of nitrogen removal, which also accelerates the membrane-fouling rate due to higher microbial metabolic production. Denitrification behavior conducted by microorganisms attached on the membrane under lower DO conditions also affected the membrane-fouling propensity.

Acknowledgments

This work was financially supported by Hebei Provincial Natural Science Fund Project (E2016402017), Colleges and Universities in Hebei Province Science and Technology Research Projects (QN2015115), Handan Science and Technology Research and Development Plan (1623209044).

References

[1] X. Huang, W.Y. Dong, H.J. Wang, S.L. Jiang, Biological nutrient removal and molecular biological characteristics in an anaerobic-multistage anaerobic/oxic (A-MAO) process to treat municipal wastewater, Bioresour. Technol., 241 (2017) 969–978.
[2] Q. Tian, L.J. Zhuang, S.K. Ong, Q. Wang, K.W. Wang, X.H. Xie, Y.B. Zhu, F. Li, Phosphorus (P) recovery coupled with increasing influent ammonium facilitated intracellular carbon source storage and simultaneous aerobic phosphorus and nitrogen removal, Water Res., 119 (2017) 267–275.
[3] S.J. Ge, Y.Z. Peng, S.Y. Wang, J.H. Guo, B. Ma, L. Zhang, X. Cao, Enhanced nutrient removal in a modified step feed process treating municipal wastewater with different inflow distribution ratios and nutrient ratios, Bioresour. Technol., 101 (2010) 9012–9019.
[4] J. Guerrero, A. Guisasola, J.A. Baeza, The nature of the carbon source rules the competition between PAO and denitrifiers in systems for simultaneous biological nitrogen and phosphorus removal, Water Res., 45 (2011) 4793–4802.
[5] S.J. Judd, The status of industrial and municipal effluent treatment with membrane bioreactor technology, Chem. Eng. J., 305 (2016) 37–45.
[6] Y.C. Woo, J.J. Lee, W.G. Shim, H.K. Shon, L.D. Tijing, M.W. Yao, H.S. Kim, Effect of powdered activated carbon on integrated submerged membrane bioreactor—nanofiltration process for wastewater reclamation, Bioresour. Technol., 210 (2016) 18–25.
[7] F.G. Meng, S.R. Chae, A. Drews, M. Kraume, H.S. Shin, F.L. Yang, Recent advances in membrane bioreactors (MBRs): membrane fouling and membrane material, Water Res., 43 (2009) 1489–1512.
[8] K.B. Melhem, Z.A. Qodah, M.A. Shannag, A. Qasaimeh, M.R. Qtaishat, M. Alkasrawi, On the performance of real grey water treatment using a submerged membrane bioreactor system, J. Membr. Sci., 476 (2015) 40–49.
[9] M. Paetkau, N. Cicek, Comparison of nitrogen removal and sludge characteristics between a conventional and a simultaneous nitrification–denitrification membrane bioreactor, Desalination, 283 (2011) 165–168.
[10] Z. Geng, E.R. Hall, P.R. Bérubé, Membrane fouling mechanisms of a membrane enhanced biological phosphorus removal process, J. Membr. Sci., 296 (2007) 93–101.
[11] C. Ratanatamskul, J. Katasomboon, Effect of sludge recirculation pattern on biological nutrient removal by a prototype IT/BF-MBR (inclined tube/biofilm-membrane bioreactor) and microbial population characteristics, Int. Biodeterior. Biodegrad., 124 (2017) 26–35.
[12] P.L. Clech, V. Chen, T.A.G. Fane, Fouling in membrane bioreactors used in wastewater treatment, J. Membr. Sci., 284 (2006) 17–53.
[13] J.R. Chen, H.J. Lin, L.G. Shen, Y.M. He, M.J. Zhang, B.Q. Liao, Realization of quantifying interfacial interactions between a randomly rough membrane surface and a foulant particle, Bioresour. Technol., 226 (2017) 220–228.
[14] I.S. Chang, P.L. Clech, B. Jefferson, S. Judd, Membrane fouling in membrane bioreactors for wastewater treatment, J. Environ. Eng., 128 (2002) 1018–1029.
[15] X. Cai, M.J. Zhang, L.N. Yang, H.J. Lin, X.L. Wu, Y.M. He, L.G. Shen, Quantification of interfacial interactions between a rough sludge floc and membrane surface in a membrane bioreactor, J. Colloid Interface Sci., 490 (2017) 710–718.
[16] L.G. Shen, Q. Lei, J.R. Chen, H.C. Hong, Y.M. He, H.J. Lin, Membrane fouling in a submerged membrane bioreactor: impacts of floc size, Chem. Eng. J., 269 (2015) 328–334.
[17] J.R. Chen, M.J. Zhang, F.Q. Li, L. Qian, H.J. Lin, L.N. Yang, X.L. Wu, X.L. Zhou, Y.M. He, B.Q. Liao, Membrane fouling in a membrane bioreactor: high filtration resistance of gel layer and its underlying mechanism, Water Res., 102 (2016) 82–89.
[18] M.J. Zhang, H.J. Lin, L.G. Shen, B.Q. Liao, X.L. Wu, R.J. Li, Effect of calcium ions on fouling properties of alginate solution and its mechanisms, J. Membr. Sci., 525 (2017) 320–329.
[19] Z. Ahmed, B.R. Lim, J.W. Cho, K.G. Song, K.P. Kim, K.H. Ahn, Biological nitrogen and phosphorus removal and changes in microbial community structure in a membrane bioreactor: effect of different carbon sources, Water Res., 42 (2008) 198–210.
[20] S.P. Feng, N.N. Zhang, H.C. Liu, X.L. Du, Y.L. Liu, H. Lin, The effect of COD/N ratio on process performance and membrane fouling in a submerged bioreactor, Desalination, 285 (2012) 232–238.
[21] M.K. Jørgensen, M. Nierychlo, A.H. Nielsen, P. Larsen, M.L. Christensen, P.H. Nielsen, Unified understanding of physico-chemical properties of activated sludge and fouling propensity, Water Res., 120 (2017) 117–132.
[22] G. Sabia, M. Ferraris, A. Spagni, Online monitoring of MBR fouling by transmembrane pressure and permeability over a long-term experiment, Sep. Purif. Technol., 122 (2014) 297–305.
[23] J.Y. Kim, I.S. Chang, H.H. Park, C.Y. Kim, J.B. Kim, J.H. Oh, New configuration of a membrane bioreactor for effective control of membrane fouling and nutrients removal in wastewater treatment, Desalination, 230 (2008) 153–161.
[24] A. Farquharson, H. Zhou, Relationships of activated sludge characteristics to fouling rate and critical flux in membrane bioreactors for wastewater treatment, Chemosphere, 79 (2010) 149–155.
[25] APHA, Standard Methods for Water and Wastewater Examination, American Public Health Association, Washington, D.C., USA, 1998.
[26] B. Frølund, R. Palmgren, K. Keiding, P.H. Nielsen, Extraction of extracellular polymers from activated sludge using a cation exchange resin, Water Res., 30 (1996) 1749–1758.
[27] S. Arabi, G. Nakhla, Characterization of foulants in conventional and simultaneous nitrification and denitrification membrane bioreactors, Sep. Purif. Technol., 69 (2009) 153–160.

[28] M. Henze, W. Gujer, T. Mino, M.C.M. van Loosdrecht, Activated Sludge 529 Models ASM1, ASM2, ASM2d and ASM3 Scientific and Technical Report No. 9, IWA Publishing, London, 2000.
[29] W. Zeng, L. Li, Y.Y. Yang, X.D. Wang, Y.Z. Peng, Denitrifying phosphorus removal and impact of nitrite accumulation on phosphorus removal in a continuous anaerobic–anoxic–aerobic (A^2O) process treating domestic wastewater, Enzyme Microb. Technol., 48 (2011) 134–142.
[30] Z.M. Fu, F.L. Yang, F.F. Zhou, Y. Xue, Control of COD/N ratio for nutrient removal in a modified membrane bioreactor (MBR) treating high strength wastewater, Bioresour. Technol., 100 (2009) 136–141.
[31] T. Kuba, E. Murnleitner, M.C.M. van Loosdrecht, J.J. Heijnen, A metabolic model for biological phosphorus removal by denitrifying organisms, Biotechnol. Bioeng., 52 (1996) 685–695.
[32] H.J. Lin, W. Peng, M.J. Zhang, J.R. Chen, H.C. Hong, Y. Zhang, A review on anaerobic membrane bioreactors: applications, membrane fouling and future perspectives, Desalination, 314 (2013) 169–188.
[33] H.J. Lin, W.J. Gao, F.G. Meng, B.Q. Liao, K.T. Leung, L.H. Zhao, J.R. Chen, H.C. Hong, Membrane bioreactors for industrial wastewater treatment: a critical review, Crit. Rev. Environ. Sci. Technol., 42 (2012) 677–740.
[34] B.M. Wiléna, P. Balmérb, The effect of dissolved oxygen concentration on the structure, size distribution of activated sludge flocs, Water Res., 33 (1999) 391–400.
[35] M.G. Kim, G. Nakhla, Comparative studies on membrane fouling between two membrane-based biological nutrient removal systems, J. Membr. Sci., 331 (2009) 91–99.
[36] V. Matějů, S. Čižinská, J. Krejčí, T. Janoch, Biological water denitrification—a review, Enzyme Microb. Technol., 14 (1992) 170–183.